CONSERVATIVE AND NON-CONSERVATIVE METHODS BASED ON HERMITE WEIGHTED ESSENTIALLY-NON-OSCILLATORY RECONSTRUCTION FOR VLASOV EQUATIONS

CHANG YANG* AND FRANCIS FILBET†

Abstract. We develop weighted essentially non-oscillatory reconstruction techniques based on Hermite interpolation both for semi-Lagrangian and finite difference methods. We apply these methods to transport equations in the context of plasma physics and the numerical simulation of turbulence phenomena. On the one hand the non-conservative semi-Lagrangian methods with high order reconstructions are particularly efficient and accurate in linear phase of simulations before the appearance of small structures. However in the non-linear phase, the lack of conservations may generate inaccurate numerical simulations. At contrast, the conservative finite difference methods are more stable in non-linear phase and the Hermite WENO reconstruction avoid spurious oscillations.

Keywords. Finite difference method; semi-Lagrangian scheme; Hermite WENO reconstruction; Vlasov-Poisson model; Guiding-center model; Plasma physics.

Contents

1. Introduction

Turbulent magnetized plasmas are encountered in a wide variety of astrophysical situations like the solar corona, accretion disks, etc, but also in magnetic fusion devices such as tokamaks. In practice, the study of such plasmas requires solving the Maxwell equations coupled to the computation of the plasma response. Different ways are possible to compute this response: the fluid or the kinetic description. Unfortunately the fluid approach seems to be insufficient when one wants to study the behavior of zonal flow, the interaction between waves and particles or the occurrence of turbulence in magnetized plasmas for example. Most of the time these plasmas are weakly collisional, and then they require a kinetic description represented by the Vlasov-Maxwell system. The numerical simulation of the full Vlasov equation involves the discretization of the six-dimensional phase space $(\mathbf{x}, \mathbf{v}) \in \mathbb{R}^3 \times \mathbb{R}^3$, which is still a challenging issue. In the context of strongly magnetized plasmas however, the motion

The authors are partially supported by the European Research Council ERC Starting Grant 2009, project 239983-*NuSiKiMo* and the Inria project Kaliffe.

* Department of Mathematics, Harbin Institute of Technology, Harbin 150001, China. (yangchang@hti.edu.cn)
† Université de Lyon & Inria, Institut Camille Jordan, EPI Kaliffe, 43 boulevard 11 novembre 1918, F-69622 Villeurbanne cedex, FRANCE. (filbet@math.univ-lyon1.fr).

of the particles is particular since it is confined around the magnetic field lines; the frequency of this cyclotron motion is faster than the frequencies of interest. Therefore, the physical system can be reduced to four or five dimensions by averaging over the gyroradius of charged particles (See for a review [1, 15]).

To develop accurate and stable numerical techniques for plasma turbulence (4D drift kinetic, 5D gyrokinetic and 6D kinetic models) is one of our long term objectives. Of course, there are already a large variety of numerical methods based on direct numerical simulation techniques. The Vlasov equation is discretized in phase space using either semi-Lagrangian [9, 10, 29, 30], finite element [18], finite difference [31] or discontinuous Galerkin [7, 20] schemes. Most of these methods are based on a time splitting discretization which is particularly efficient for classical Vlasov-Poisson or Vlasov-Maxwell systems since the characteristic curves corresponding to the split operator simply become straight lines and can be solved exactly. Therefore, the numerical error is only due to the splitting in time and the phase space discretization of the distribution function. Furthermore for such time splitting schemes, the semi-Lagrangian methods on Cartesian grids coupled with Lagrange, Hermite or cubic spline interpolation techniques are conservative [3, 10]. Hence, these methods are now currently used and have proven their efficiency for various applications and in this context they are often observed to be less dissipative than classical finite volume or finite difference schemes. However, for more elaborated kinetic equations like the 4D drift kinetic [16] or 5D gyrokinetic [17] equations, or even the two dimensional guiding center model [30], time splitting techniques cannot necessarily be applied. Thus characteristic curves are more sophisticated and required a specific time discretization. For instance, in [16, 17] several numerical solvers have been developed using an Eulerian formulation for gyro-kinetic models. However, spurious oscillations often appear in the non-linear phase when small structures occur and it is difficult to distinguish physical and numerical oscillations. Moreover, for these models semi-Lagrangian methods are no more conservative, hence the long time behavior of the numerical solution may become unsuitable.

For this purpose, we want to develop a class of numerical methods based on the Hermite interpolation which is known to be less dissipative than Lagrange interpolation [10] together with a weighted essentially non-oscillatory (WENO) reconstruction applied to semi-Lagrangian and finite difference methods. Actually, Hermite interpolation with WENO schemes were already studied in [26] in the context of discontinuous Galerkin methods with slope limiters. A system of equations for the unknown function and its first derivative is evolved in time and used in the reconstruction. Moreover, a similar technique, called CIP (Cubic Interpolation Propagation), has also been proposed for transport equations in plasma physics applications [24], but the computational cost is strongly increased since the unknown and all the derivatives are advected in phase space. In [10], a semi-Lagrangian method with Hermite interpolation has been proposed and shown to be efficient and less dissipative than Lagrangian interpolation. In this method, the first derivatives are approximated by a fourth order centered finite difference formula.

Here, we also apply a similar pseudo-Hermite reconstruction [10] and meanwhile introduce an appropriate WENO reconstruction to control spurious oscillation leading to nonlinear schemes. We develop third and fifth order methods and apply them to semi-Lagrangian (non-conservative schemes) and conservative finite difference methods. Our numerical results will be compared to the usual semi-Lagrangian method with cubic spline interpolation [30] and the classical fifth order WENO finite difference scheme [22].

The paper is organized as follows : we first present the Vlasov equation and related models which will be investigated numerically. Then in section 3, the semi-Lagrangian method is proposed with high order Hermite interpolation with a WENO reconstruction to control spurious oscillations. In section 4, conservative finite difference schemes with Hermite WENO reconstructions are detailed. In section 5, a discussion of approximation of first derivatives is

presented. Then the one-dimensional free transport equation with oscillatory initial data is investigated to compare our schemes with classical ones (semi-Lagrangian with cubic spline interpolation and conservative finite difference schemes with WENO reconstruction). Finally we perform numerical simulations on the simplified paraxial Vlasov-Poisson model and on the guiding center model for highly magnetized plasma in two dimension.

2. The Vlasov equation and related models

The evolution of the density of particles $f(t,\mathbf{x},\mathbf{v})$ in the phase space $(\mathbf{x},\mathbf{v}) \in \mathbb{R}^d \times \mathbb{R}^d$, $d = 1,..,3$, is given by the Vlasov equation,

$$\frac{\partial f}{\partial t} + \mathbf{v}\cdot\nabla_{\mathbf{x}} f + \mathbf{F}(t,\mathbf{x},\mathbf{v})\cdot\nabla_{\mathbf{v}} f = 0, \tag{2.1}$$

where the force field $F(t,\mathbf{x},\mathbf{v})$ is coupled with the distribution function f giving a nonlinear system. We mention the well known Vlasov-Poisson (VP) model describing the evolution of particles under the effects of self-consistent electro-magnetic fields. We define the charge density $\rho(t,x)$ by

$$\rho(t,\mathbf{x}) = q\int_{\mathbb{R}^d} f(t,\mathbf{x},\mathbf{v})\,d\mathbf{v}, \tag{2.2}$$

where q is the single charge. The force field is given for the Vlasov-Poisson model by

$$\mathbf{F}(t,\mathbf{x},\mathbf{v}) = \frac{q}{m}\mathbf{E}(t,\mathbf{x}), \quad \mathbf{E}(t,\mathbf{x}) = -\nabla_{\mathbf{x}}\phi(t,\mathbf{x}), \quad -\Delta_{\mathbf{x}}\phi = \frac{\rho}{\varepsilon_0}, \tag{2.3}$$

where m represents the mass of one particle. These equations and related reduced equations, such as 4D drift-kinetic equation [19], are frequently used to describe plasma turbulence in a Tokamak core.

In the sequel, we will also consider the so-called 2D guiding-center model [21], which can be obtained by integrating the 4D drift-kinetic model on $z, v_{\|}$. This model can describe the evolution of the charge density in a highly magnetized plasma in the transverse plane of a tokamak, given by

$$\begin{cases} \dfrac{\partial \rho}{\partial t} + \mathbf{U}\cdot\nabla\rho = 0, \\ -\Delta\phi = \rho. \end{cases} \tag{2.4}$$

where the velocity $\mathbf{U} = (-\partial_y\phi, \partial_x\phi)$ is divergence free.

Transport equations (2.1) or (2.4) can be recast into an advective form

$$\frac{\partial f}{\partial t} + \mathbf{A}\cdot\nabla f = 0, \tag{2.5}$$

where $\mathbf{A} : \mathbb{R}^N \times \mathbb{R}^+ \to \mathbb{R}^N$, $N \geq 1$. Hence, classical backward semi-Lagrangian method can be applied to solve (2.5). Furthermore, under the assumption $\nabla\cdot\mathbf{A} = 0$, equations (2.1) or (2.4) can also be rewritten in a conservative form

$$\frac{\partial f}{\partial t} + \mathrm{div}(\mathbf{A}f) = 0, \tag{2.6}$$

for which a finite difference method can be used.

3. Hermite WENO reconstruction for semi-Lagrangian methods

We introduce a high order Hermite interpolation coupled with a weight essentially non-oscillatory (HWENO) reconstruction for semi-Lagrangian methods. The classical HWENO should evaluate the distribution function f and its spatial derivatives, which increases computational cost [26]. We thus devote to develop a more efficient HWENO scheme based on finite difference approximations of the derivatives.

The semi-Lagrangian method becomes a classical method for the numerical solution of the Vlasov equation because of its high accuracy and its small dissipation [2, 30]. Moreover, it does not constraint any restriction on the time step size. Indeed, the key issue of the semi-Lagrangian method compared to classical Eulerian schemes is that it uses the characteristic curves corresponding to the transport equation to update the unknown from one time step to another. Let us recall the main feature of the backward semi-Lagrangian method. For a given $s \in \mathbb{R}^+$, the differential system

$$\begin{cases} \dfrac{d\mathbf{X}}{dt} = \mathbf{A}(t, \mathbf{X}), \\ \mathbf{X}(s) = \mathbf{x}, \end{cases}$$

is associated to the transport equation (2.5). We denote its solution by $\mathbf{X}(t; s, \mathbf{x})$. The backward semi-Lagrangian method is decomposed into two steps for computing the function f^{n+1} at time t_{n+1} from the function f^n at time t_n :

(1) For each mesh point $\mathbf{x}_i$ of phase space, compute the backward characteristic $\mathbf{X}(t_n; t_{n+1}, \mathbf{x}_i)$, the value of the characteristic at time t_n who is equal to $\mathbf{x}_i$ at time t_{n+1}.
(2) As the function f of transport equation verifies

$$f^{n+1}(\mathbf{x}_i) = f^n(\mathbf{X}(t_n; t_{n+1}, \mathbf{x}_i)),$$

we obtain the value of $f^{n+1}(\mathbf{x}_i)$ by computing $f^n(\mathbf{X}(t_n; t_{n+1}, \mathbf{x}_i))$ by interpolation, since $\mathbf{X}(t_n; t_{n+1}, \mathbf{x}_i)$ is not usually a mesh point.

In practice, a cubic spline interpolation is often used [8, 14]. It gives very good results, but it has the drawback of being non local which causes a higher communication overhead on parallel computers. Moreover spurious oscillations may occur around discontinuities. On the other hand, the cubic Hermite interpolation is local, and has been shown in [10] to be less dissipative than Lagrange interpolation polynomial. However, it has still spurious oscillations for discontinuous solution.

Here, we develop a third and fifth order Hermite interpolation coupled with a weighted essentially non-oscillatory procedure, such that it is accurate for smooth solutions and it removes spurious oscillations around discontinuities or high frequencies which cannot be solved on a fixed mesh.

3.1. **Third order Hermite WENO reconstruction in 1D.** Consider a uniform mesh $(x_i)_i$ of the computational domain and assume that the values of the distribution function $(f_i)_i$ and its derivative $(f_i')_i$ are known at the grid points. The standard cubic Hermite polynomial $H_3(x)$ on the interval $I_i = [x_i, x_{i+1}]$ can be expressed as follows :

$$\begin{aligned} H_3(x) &= f_i + \frac{f_{i+1} - f_i}{\Delta x}(x - x_i) + \frac{(f_{i+1} - f_i) - \Delta x f_i'}{\Delta x^2}(x - x_i)(x - x_{i+1}) \\ &\quad + \frac{\Delta x(f_i' + f_{i+1}') - 2(f_{i+1} - f_i)}{\Delta x^3}(x - x_i)^2(x - x_{i+1}). \end{aligned} \tag{3.1}$$

The polynomial $H_3(x)$ verifies :

$$\begin{cases} H_3(x_i) = f_i, & H_3'(x_i) = f_i', \\ H_3(x_{i+1}) = f_{i+1}, & H_3'(x_{i+1}) = f_{i+1}'. \end{cases}$$

Moreover, we define two quadratic polynomials in the interval I_i :

$$h_l(x) = f_i + \frac{f_{i+1} - f_i}{\Delta x}(x - x_i) + \frac{(f_{i+1} - f_i) - \Delta x f_i'}{\Delta x^2}(x - x_i)(x - x_{i+1}), \tag{3.2}$$

$$h_r(x) = f_i + \frac{f_{i+1} - f_i}{\Delta x}(x - x_i) + \frac{\Delta x f_{i+1}' - (f_{i+1} - f_i)}{\Delta x^2}(x - x_i)(x - x_{i+1}). \tag{3.3}$$

The polynomial of degree 2 h_l verifies

$$h_l(x_i) = f_i, \quad h_l(x_{i+1}) = f_{i+1}, \quad h_l'(x_i) = f_i',$$

while h_r verifies

$$h_r(x_i) = f_i, \quad h_r(x_{i+1}) = f_{i+1}, \quad h_r'(x_{i+1}) = f_{i+1}'.$$

The idea of WENO reconstruction is now to use the cubic polynomial H_3 when function f is smooth, otherwise, we use the less oscillatory polynomial of degree 2 between h_l or h_r. Thus, let us write H_3 as follows

$$H_3(x) \;=\; w_l(x)\, h_l(x) \;+\; w_r(x)\, h_r(x),$$

where w_l and w_r are WENO weights. When the function f is smooth, we expect that

$$w_l(x) \approx c_l(x) = \frac{x_{i+1} - x}{\Delta x} \quad \text{and} \quad w_r(x) \approx c_r(x) = 1 - c_l(x),$$

so that we recover the third order Hermite polynomial. Otherwise, we expect that

$$w_l(x) \approx 1, w_r(x) \approx 0 \quad \text{or} \quad w_l(x) \approx 0, w_r(x) \approx 1 \tag{3.4}$$

according to the region where f is less smooth. To determine these WENO weights, we follow the strategy given in [22] and first define smoothness indicators by integration of the first and second derivatives of h_l and h_r on the interval I_i :

$$\beta_l \;=\; \int_{x_i}^{x_{i+1}} \Delta x (h_l')^2 + \Delta x^3 (h_l'')^2 dx \;=\; (f_i - f_{i+1})^2 + \frac{13}{3}((f_{i+1} - f_i) - \Delta x f_i')^2,$$

$$\beta_r \;=\; \int_{x_i}^{x_{i+1}} \Delta x (h_r')^2 + \Delta x^3 (h_r'')^2 dx \;=\; (f_i - f_{i+1})^2 + \frac{13}{3}(\Delta x f_{i+1}' - (f_{i+1} - f_i))^2.$$

Then we set w_l and w_r as

$$w_l(x) = \frac{\alpha_l(x)}{\alpha_l(x) + \alpha_r(x)} \quad \text{and} \quad w_r(x) = 1 - w_l(x),$$

where

$$\alpha_l(x) = \frac{c_l(x)}{(\varepsilon + \beta_l)^2} \quad \text{and} \quad \alpha_r(x) = \frac{c_r(x)}{(\varepsilon + \beta_r)^2}.$$

where $\varepsilon = 10^{-6}$ to avoid the denominator to be zero.

Observe that when the function f is smooth, the difference between β_l and β_r becomes small and the weights $w_l(x) \approx c_l(x)$ and $w_r(x) \approx c_r(x)$. Otherwise, when the smoothness indicator β_s, $s = l, r$ blows-up, then the parameter α_s and the weight w_s goes to zero, which yields (3.4).

Finally, let us mention that the following fourth-order centred finite difference formula is used to approximate the first derivative at the grid point x_i

$$f_i' = \frac{1}{12\Delta x}(f_{i-2} - 8f_{i-1} + 8f_{i+1} - f_{i+2}). \tag{3.5}$$

However, other choices may be done and a further discussion on the different possibilities will be given in section 5.1.

Now, we give an error estimate on the Hermite WENO interpolation procedure and compare it with the classical WENO interpolation based on Lagrange interpolation.

Proposition 3.1. *Assuming that f is smooth, we can formally prove that*

$$E^H(r) = f(x) - H_3(x) = \frac{f^{(4)}(x_i)}{4!} r^2 (1 - r)^2 \Delta x^4 + O(\Delta x^5), \tag{3.6}$$

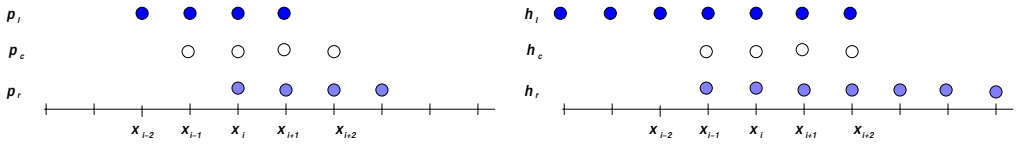

FIGURE 1. Stencil used for the (a) fifth order classical WENO interpolation and (b) fifth order Hermite WENO interpolation with sixth order finite difference approximation of the first derivative

where $0 \leq r = \frac{x-x_i}{\Delta x} \leq 1$. *This approximation error* $E_H(r)$ *is smaller than that of cubic Lagrange reconstruction* $L_3(x)$

$$E^L(r) = f(x) - L_3(x) = \frac{f^{(4)}(x_i)}{4!}(1+r)r(1-r)(2-r)\Delta x^4 + O(\Delta x^5). \tag{3.7}$$

From this proposition, we observe that the amplitude of the error of the Hermite reconstruction is smaller than the one obtained from a Lagrange interpolation.

Remark 3.2. *We emphasize that the coefficients* $\frac{f^{(4)}(x_i)}{4!}r^2(1-r)^2$ *in the error estimate* (3.6) *is guaranteed by fourth or higher order approximation of the derivative. On the opposite, a lower order approximation would affect this coefficients, and thus the error amplitude.*

Remark 3.3. *Hermite and Lagrange WENO procedures have the same complexity since the discrete derivative can be computed and stored before the reconstruction step. Indeed, we have 27 additions (resp. 32) and 47 (resp. 44) multiplications for the Lagrange WENO (resp. Hermite WENO) procedure.*

On the other hand, as we show in Figure 1, the stencils for the Hermite WENO reconstruction with a centred approximation of the first order derivative is much wider than the one for the Lagrange WENO reconstruction. Moreover, for the HWENO procedure, the intersection of the reconstruction points of h_l, h_c *and* h_r *is* $\{x_{i-1}, x_i, x_{i+1}, x_{i+2},\}$ *whereas it is only* $\{x_i, x_{i+1}\}$ *for WENO. Hence, we should expect some spurious oscillations when a discontinuity is located on* (x_{i-1}, x_{i+2}). *This issue may be fixed using a decentred approximation of the derivative on each side. However, numerical simulations performed in section 5.1 show that the centered approximation is the most robust and accurate.*

3.2. **Fifth order Hermite WENO reconstruction.** We can extend previous method to a fifth order Hermite WENO reconstruction. In the same way, we first construct a fifth degree polynomial $H_5(x)$ on the interval $[x_i, x_{i+1}]$

$$H_5(x_j) = f_j,\ j = i-1,\ i,\ i+1, i+2, \quad H_5'(x_{i-1}) = f_{i-1}',\ H_5'(x_{i+2}) = f_{i+2}'$$

and then polynomials of degree three $h_l(x)$, $h_c(x)$, $h_r(x)$ verifying

$$\begin{cases} h_l(x_j) = f_j, \quad j = i-1,\ i,\ i+1, & h_l'(x_{i-1}) = f_{i-1}', \\ h_c(x_j) = f_j, \quad j = i-1,\ i,\ i+1,\ i+2, & \\ h_r(x_j) = f_j, \quad j = i, i+1, i+2, & h_r'(x_{i+2}) = f_{i+2}', \end{cases}$$

where the first derivative f_i' is given by a sixth order centered approximation

$$f_i' = \frac{1}{60}[(f_{i+3} - f_{i-3}) - 9(f_{i+2} - f_{i-2}) + 45(f_{i+1} - f_{i-1})].$$

Then the polynomial H_5 can be written as a convex combination

$$H_5(x) \ = \ w_l(x)h_l(x) + w_c(x)h_c(x) + w_r(x)h_r(x),$$

where $w_l(x)$, $w_c(x)$, $w_r(x)$ are WENO weights depending on x. Similarly smoothness indicators are computed by integration of the first, second and third order derivatives of $h_l(x)$, $h_c(x)$, $h_r(x)$ on the interval $[x_i, x_{i+1}]$:

$$\beta_j = \int_{x_i}^{x_{i+1}} \Delta x (h_j')^2 + \Delta x^3 (h_j'')^2 + \Delta x^5 (h_j''')^2 dx, \quad j = l, c, r.$$

Finally, the WENO weights are determined according to the smoothness indicators

$$\begin{cases} w_l(x) = \dfrac{\alpha_l(x)}{\alpha_l(x)+\alpha_c(x)+\alpha_r(x)}, & \alpha_l(x) = \dfrac{c_l(x)}{(\varepsilon+\beta_l)^2}, \quad c_l(x) = \dfrac{(x-x_{i+2})^2}{9\Delta x^2}, \\ w_c(x) = \dfrac{\alpha_c(x)}{\alpha_l(x)+\alpha_c(x)+\alpha_r(x)}, & \alpha_c(x) = \dfrac{c_c(x)}{(\varepsilon+\beta_c)^2}, \quad c_c(x) = 1 - c_l(x) - c_r(x), \\ w_r(x) = \dfrac{\alpha_r(x)}{\alpha_l(x)+\alpha_c(x)+\alpha_r(x)}, & \alpha_r(x) = \dfrac{c_r(x)}{(\varepsilon+\beta_r)^2}, \quad c_r(x) = \dfrac{(x-x_{i-1})^2}{9\Delta x^2}. \end{cases}$$

This polynomial reconstruction allow to get fifth order accuracy for smooth stencil and the various stencils are expected to damp oscillations when filamentation of the distribution function occurs. Finally, let us observe that this technique can be easily extended to high space dimension on Cartesian grids.

4. Hermite WENO reconstruction for conservative finite difference methods

When the velocity $\mathbf{A}$ is not constant in (2.5), the semi-Lagrangian method is not conservative even when $\mathrm{div}\mathbf{A} = 0$, hence mass is no longer conserved and the long time behavior of the numerical solution may be wrong even for small time steps. Therefore, high order conservative methods may be more appropriate even if they are restricted by a CFL condition. An alternative is to use the finite difference formulation in the conservative form and to use the semi-Lagrangian method for the flux computation [27, 28].

In this section, we extend Hermite WENO reconstruction for computing numerical flux of finite difference method. For instance we consider the one dimensional transport equation

$$\frac{\partial f}{\partial t} + \frac{\partial}{\partial x}(Af) = 0,$$

We set $u = Af$ and suppose that $\{u_i\}_{1\le i\le N}$ is approximation of $u(x_i)$, where u is a smooth function. We look for $\{\hat{f}_{i+1/2}\}_{0\le i\le N}$ such that the flux difference approximates the derivative $u'(x)$ to k-th order accuracy :

$$\frac{\hat{f}_{i+1/2} - \hat{f}_{i-1/2}}{\Delta x} = u'(x) + \mathcal{O}(\Delta x^k).$$

An upwind scheme gives

$$\hat{f}_{i+1/2} = \begin{cases} \hat{f}^l_{i+1/2}, & \text{if } A(x_{i+1/2}) > 0, \\ \hat{f}^r_{i+1/2},, & \text{else,} \end{cases}$$

where $\hat{f}^l_{i+1/2}$ (resp. $\hat{f}^r_{i+1/2}$) is the numerical flux reconstructed on the left (resp. right) hand side.

Then, let us define a function g such that

$$u(x) = \frac{1}{\Delta x}\int_{x-\Delta x/2}^{x+\Delta x/2} g(s)ds, \tag{4.1}$$

then clearly

$$u'(x) = \frac{1}{\Delta x}\left[g(x+\Delta x/2) - g(x-\Delta x/2)\right].$$

Hence we define the flux function $\hat{f}_{i+1/2}$ as an approximation of $g(x_i + \Delta x/2)$. Let us denote by G one primitive of g

$$G(x) = \int_{-\infty}^{x} g(s)ds,$$

then (4.1) implies

$$G(x_{i+1/2}) = \sum_{j=-\infty}^{i} \int_{x_{j-1/2}}^{x_{j+1/2}} g(s)ds = \Delta x \sum_{j=-\infty}^{i} u_j := G_{i+1/2}.$$

Thus, given the point values $\{u_i\}$, the primitive function $G(x)$ is exactly known at $x = x_{i+1/2}$. We thus can approximate $G(x)$ by an interpolation method. Therefore,

$$g(x_{i+1/2}) = \left.\frac{dG}{dx}\right|_{x=x_{i+1/2}}. \tag{4.2}$$

Now let us interpolate the primitive function $G(x)$. Here we only consider high order Hermite WENO scheme and outline the procedure of reconstruction only for the fifth order accuracy case.

The aim is to construct an approximation of the flux $\hat{f}_{i+1/2}$ by the Hermite polynomial of degree five together with a WENO reconstruction from point values $\{u_i\}$. For instance here we choose to present the left hand side reconstruction on the interval $(x_{i-1/2}, x_{i+1/2})$:

(1) We construct the Hermite polynomial H_5 such that

$$H_5(x_{i+j+1/2}) = G_{i+j+1/2},\ j = -2, -1, 0, 1, \quad H_5'(x_{i+j+1/2}) = G'_{i+j+1/2},\ j = -2, 1,$$

(2) We construct cubic reconstruction polynomials $H_l(x)$, $H_c(x)$, $H_r(x)$ such that :

$$\begin{cases} H_l(x_{i+j+1/2}) = G_{i+j+1/2},\ j = -2, -1, 0, & H_l'(x_{i-3/2}) = G'_{i-3/2}, \\ H_c(x_{i+j+1/2}) = G_{i+j+1/2},\ j = -2, -1, 0, 1, & \\ H_r(x_{i+j+1/2}) = G_{i+j+1/2},\ j = -1, 0, 1, & H_r'(x_{i+3/2}) = G'_{i+3/2}, \end{cases}$$

where $G'_{i+1/2}$ is the sixth order centered approximation of first derivative

$$G'_{i+1/2} = \frac{1}{60}[(u_{i+3} - u_{i-2}) - 8(u_{i+2} - u_{i-1}) + 37(u_{i+1} - u_i)].$$

Let us denote by $h_l(x)$, $h_c(x)$, $h_r(x)$, $h_5(x)$ the first derivatives of $H_l(x)$, $H_c(x)$, $H_r(x)$, $H_5(x)$ respectively. By evaluating $h_l(x)$, $h_c(x)$, $h_r(x)$, $h_5(x)$ at $x = x_{i+1/2}$, we obtain

$$h_5(x_{i+1/2}) = \frac{-8u_{i-1} + 19u_i + 19u_{i+1} + 3G'_{i-3/2} - 6G'_{i+3/2}}{27}$$

and

$$\begin{aligned} h_l(x_{i+1/2}) &= -2\,u_{i-1} + 2u_i + G'_{i-3/2}, \\ h_c(x_{i+1/2}) &= \frac{-u_{i-1} + 5\,u_i + 2\,u_{i+1}}{6}, \\ h_r(x_{i+1/2}) &= \frac{u_i + 5\,u_{i+1} - 2\,G'_{i+3/2}}{4}. \end{aligned}$$

(3) We evaluate the smoothness indicators β_l, β_c, β_r, which measure the smoothness of $h_l(x)$, $h_c(x)$, $h_r(x)$ on the cell $[x_i, x_{i+1}]$.

$$\begin{aligned}
\beta_l &= \int_{x_i}^{x_{i+1}} \Delta x (h_l'(x))^2 + \Delta x^3 (h_l''(x))^2 dx \\
&= l_1^2 + 3\, l_1\, l_2 + \frac{75}{16} l_2^2, \quad \text{with } l_1 = u_i - u_{i-1}, \quad l_2 = -3u_{i-1} + u_i + 2G'_{i-3/2}, \\
\beta_c &= \int_{x_i}^{x_{i+1}} \Delta x (h_c'(x))^2 + \Delta x^3 (h_c''(x))^2 dx \\
&= c_1^2 + 2\, c_1\, c_2 + \frac{25}{12} c_2^2, \quad \text{with } c_1 = u_i - u_{i-1}, \quad c_2 = u_{i-1} - 2u_i + u_{i+1}, \\
\beta_r &= \int_{x_i}^{x_{i+1}} \Delta x (h_r'(x))^2 + \Delta x^3 (h_r''(x))^2 dx \\
&= r_1^2 + 3\, r_1\, r_2 + \frac{39}{16} r_2^2, \quad \text{with } r_1 = u_{i+1} - u_i, \quad r_2 = u_i - 3u_{i+1} + 2G'_{i+3/2}.
\end{aligned}$$

(4) We compute the non-linear weights based on the smoothness indicators

$$\begin{cases}
w_l = \dfrac{\alpha_l}{\alpha_l + \alpha_c + \alpha_r}, & \alpha_l = \dfrac{c_l}{(\varepsilon + \beta_l)^2}, \\
w_c = \dfrac{\alpha_c}{\alpha_l + \alpha_c + \alpha_r}, & \alpha_c = \dfrac{c_c}{(\varepsilon + \beta_c)^2}, \\
w_r = \dfrac{\alpha_r}{\alpha_l + \alpha_c + \alpha_r}, & \alpha_r = \dfrac{c_r}{(\varepsilon + \beta_r)^2},
\end{cases}$$

where the coefficients $c_l = 1/9$, $c_c = 4/9$, $c_r = 4/9$ are chosen to get fifth order accuracy for smooth solutions and the parameter $\varepsilon = 10^{-6}$ avoids the blow-up of α_k, $k = \{l, c, r\}$.

(5) The flux $\hat{f}^l_{i+1/2}$ is then computed as

$$\hat{f}^l_{i+1/2} = w_l\, h_l(x_{i+1/2}) + w_c\, h_c(x_{i+1/2}) + w_r\, h_r(x_{i+1/2}).$$

The reconstruction to $\hat{f}^r_{i+1/2}$ is mirror symmetric with respect to $x_{i+1/2}$ of the above procedure.

5. Numerical simulation of Vlasov equation and related models

We start with a discussion of approximation of first derivatives for Hermite WENO reconstruction. Then we check the order of accuracy and compare the error amplitude of the various numerical schemes with a very basic test on the one dimensional transport equation with constant velocity. Finally we perform numerical simulations on the simplified paraxial Vlasov-Poisson model and on the guiding center model for highly magnetized plasma in the transverse plane of a tokamak.

In this section we will compare our Hermite WENO reconstruction with the usual semi-Lagrangian method with cubic spline interpolation without splitting [30], and with the classical fifth order finite difference technique [22] coupled with a fourth order Runge-Kutta scheme for the time discretization.

5.1. A discussion on approximation of f_i'.

In section 3.1, we have proposed a fourth-order centred finite difference formula (3.5) for f_i' in third order Hermite WENO reconstruction. However, in this subsection, different approximations of f_i' will be compared.

Let us only consider f_i' in $h_l(x)$ of (3.2), then following approximations will be considered

- Second-order centred approximation

$$f_i' = \frac{1}{2\Delta x}(-f_{i-1} + f_{i+1}).$$

- Fourth-order WENO approximation

$$f_i' = w_l f_l' + w_c f_c' + w_r f_r',$$

where w_l, w_c, w_r are WENO type weights, f_l', f_c', f_r' are third-order decentred approximation

$$\begin{aligned} f_l' &= \frac{1}{2\Delta x}(f_{i-2} - 4f_{i-1} + 3f_i), \\ f_c' &= \frac{1}{2\Delta x}(-f_{i-1} + f_{i+1}), \\ f_r' &= \frac{1}{2\Delta x}(-3f_i + 4f_{i+1} - f_{i+2}). \end{aligned}$$

- Fourth-order centred approximation

$$f_i' = \frac{1}{12\Delta x}(f_{i-2} - 8f_{i-1} + 8f_{i+1} - f_{i+2}).$$

- Sixth-order centred approximation

$$f_i' = \frac{1}{60\Delta x}(-f_{i-3} + 9f_{i-2} - 45f_{i-1} + 45f_{i+1} - 9f_{i+2} + f_{i+3}).$$

For comparison, let us consider the free transport equation

$$\frac{\partial f}{\partial t} + \frac{\partial f}{\partial x} = 0, \quad x \in [-1,1], \quad t \geq 0, \tag{5.1}$$

with periodic boundary conditions.

We first consider a smooth solution, where the initial condition is chosen as

$$f(0,x) = \sin(\pi x), \quad x \in [-1,1].$$

We present in Table 1 numerical errors for semi-Lagrangian-HWENO 3rd method with different approximations of f_i' in continuous solution case. We first note that all the approaches can achieve third-order actuary. The one with 2nd-order centred approximation is less precise than the others. Moreover, we notice that higher order centred approximation can no more improve the precision.

n_x	200		400		800	
	$\|\cdot\|_1$	r	$\|\cdot\|_1$	r	$\|\cdot\|_1$	r
2nd-order Centred	9.35e-6	3.02	1.164e-6	3.01	1.45e-7	3.00
4th-order WENO	1.04e-6	3.03	1.29e-7	3.01	1.62e-8	3.00
4th-order Centred	1.04e-6	3.03	1.29e-7	3.01	1.62e-8	3.00
6th-order Centred	1.04e-6	3.02	1.29e-7	3.01	1.62e-8	3.00

TABLE 1. Comparison of different first derivative approximations in continuous solution case: *Error in L^1-norm and order of convergence r. The final time is $T_{end} = 8$.*

Then we consider a discontinuous solution, a step function, as follows

$$f(0,x) = \begin{cases} 1, & \text{for } -1 \leq x \leq 0, \\ 0, & \text{otherwise.} \end{cases} \tag{5.2}$$

It is clear from table 2 that the approaches with 4th-order WENO and centred approximations are more precise than the one with 2nd-order centred approximation both for the precision and for the control of oscillation. Moreover, the approach with 4th-order centred approximation is even better than the ones with 4th-order WENO and 6th-order centred approximations, and it is cheaper in sense of computational cost then later ones. We thus propose to use the 4th-order centred approximations for the first derivatives.

The similar results can be observed in the semi-Lagrangian-HWENO 5th method and finite difference HWENO 5th method with different approximations of first derivatives.

n_x	200	400	800
2nd-order Centred	4.72e-2	2.76e-2	1.60e-2
4th-order WENO	4.39e-2	2.65e-2	1.57e-2
4th-order Centred	3.27e-2	1.89e-2	1.09e-2
6th-order Centred	3.08e-2	1.78e-2	1.03e-2

(a) Error between the exact solution and the approximated solutions

n_x	200	400	800
2nd-order Centred	3.32e-3	5.34e-3	8.21e-3
4th-order WENO	2.04e-3	2.68e-3	3.77e-3
4th-order Centred	5.71e-4	5.18e-4	4.37e-4
6th-order Centred	1.70e-3	1.99e-3	2.65e-3

(b) Error of total variation

TABLE 2. Comparison of different first derivative approximations in discontinuous solution case: *(a) Error in L^1 norm and r is the order of accuracy (b) Error on the total variation. The final time is $T_{end} = 8$.*

5.2. **1D transport equation.** In this subsection, we consider again the free transport equation (5.1), but compare our Hermite WENO reconstruction with various classical methods.

We present in Tables 3 and 4, the numerical error for different methods. On the one hand for semi-Lagrangian methods in Table 3, the third and fifth order Hermite WENO reconstruction are compared with the cubic spline interpolation. The semi-Lagrangian method is unconditionally stable, we thus choose a CFL number larger than one, *e.g.* $\lambda = \frac{\Delta t}{\Delta x} = 2.5$. For this equation, the time integration is exact since the characteristic curves are straight lines, hence the numerical error is only due to the accumulation of the interpolation error at each time step. For a reconstruction of degree p, the error is expected to be of order $O(\Delta x^{p+1}/\Delta t)$, that is $O(\Delta x^p/\lambda)$. We observe that the cubic spline and third order Hermite WENO reconstructions have both third order accuracy, and the numerical error has almost the same amplitude. The third order Hermite WENO reconstruction is much accurate than the classical third order WENO reconstruction, which corresponds to the approximation errors (3.6),(3.7). The semi-Lagrangian method with a fifth order Hermite WENO reconstruction has fifth order accuracy, thus it is much more accurate than the previous third order methods.

On the other hand in Table 4, we focus on the finite difference method and compare the fifth order Hermite WENO reconstruction with the classical fifth order WENO reconstruction [22]. We choose a CFL number such that the time stepping error is negligible to spatial error, *e.g.* $\lambda = \frac{\Delta t}{\Delta x} = 0.4$.. We thus observe that these two methods have fifth order accuracy, but the fifth order Hermite WENO interpolation method is much more accurate than the usual fifth order WENO method. Furthermore, for the same order of accuracy the semi-Lagrangian method

n_x	200		400		800	
	$\|\cdot\|_1$	r	$\|\cdot\|_1$	r	$\|\cdot\|_1$	r
Semi-Lagrangian cubic spline	1.03e-6	3.00	1.29e-7	3.00	1.61e-8	3.00
Semi-Lagrangian WENO 3rd	9.48e-6	3.08	1.17e-6	3.02	1.45e-7	3.00
Semi-Lagrangian HWENO 3rd	1.04e-6	3.03	1.29e-7	3.01	1.62e-8	3.00
Semi-Lagrangian WENO 5th	1.92e-9	5.02	5.98e-11	5.00	1.94e-12	4.94
Semi-Lagrangian HWENO 5th	9.28e-10	5.51	2.28e-11	5.35	8.63e-13	4.72

(a) Error between the exact solution and the approximated solutions

SL-spline	SL-WENO3	SL-HWENO3	SL-WENO5	SL-HWENO5
0.56	0.05	0.06	0.14	0.16

(b) Computational time for different methods in the case $n_x = 800$

TABLE 3. Comparison of the semi-Lagrangian methods in continuous solution case: *(a) Error in L^1-norm and order of convergence r, (b) Computational time, in seconds. The final time is $T_{end} = 8$.*

is much more precise than the finite difference scheme, which is expected for linear problems since the error only comes from the polynomial interpolation. Computational time is rather similar with both reconstructions.

n_x	200		400		800	
	$\|\cdot\|_1$	r	$\|\cdot\|_1$	r	$\|\cdot\|_1$	r
Finite difference WENO 5th	1.15e-7	4.99	3.60e-9	5.01	1.16e-10	4.95
Finite difference HWENO 5th	6.06e-8	4.99	1.92e-9	4.98	6.55e-11	4.87

(a) Error between the exact solution and the approximated solutions

FD-WENO5	FD-HWENO5
2.48	2.85

(b) Computational time for different methods in the case $n_x = 800$

TABLE 4. Comparison of the finite difference methods in continuous solution case: *(a) Error in L^1-norm and order of convergence r, (b) Computational time, in seconds. The final time is $T_{end} = 8$.*

Comparisons of the methods in discontinuous solution case are now summarized in Tables 5 and 6. We first notice that all the methods can achieve order of accuracy of $\frac{p}{p+1}$, where p is degree of polynomial. This numerical results are in perfect argument with the stability result proven in [6, Corollary 7] for discontinuous solution. Indeed, even without any limiter, the high order scheme remains stable and convergent for discontinuous solution. Surprisingly, the order of accuracy increases with the degree of polynomial. Moreover, it is clear that semi-Lagrangian methods with spline cubic and Hermite interpolations are more precise than fourth-order Runge-Kutta time discretization coupled with the finite difference methods with the different WENO reconstructions. More precisely for $n_x \leq 10^3$, the cubic spline interpolation is more accurate than Hermite polynomials of degree three and five coupled with the WENO reconstruction. It illustrates perfectly the robustness of the semi-Lagrangian method with cubic spline interpolation. Nevertheless it also generates a lot of oscillations (see Table 5 (b)) which produce negative values of the distribution function. Furthermore it seems that

the fifth order Hermite WENO reconstruction is less dissipative than usual fifth order WENO one and it is more accurate. Both of them control well spurious oscillations (see Table 5 (b)).

Here, we emphasize that the Hermite WENO reconstructions do not significantly increase the computational cost with respect to the classical WENO reconstructions (see Remark 3.3).

On the other hand, we notice that the error of the Hermite WENO reconstruction is only 50% of that of the classical WENO reconstruction in the smooth solution case, and it is about 90% in the non-smooth solution case. Therefore, the Hermite WENO reconstruction is more efficient than the classical WENO reconstruction.

n_x	200		400		800	
	$\|\cdot\|_1$	r	$\|\cdot\|_1$	r	$\|\cdot\|_1$	r
Semi-Lagrangian cubic spline	2.47e-2	0.80	1.43e-2	0.79	8.52e-3	0.75
Semi-Lagrangian WENO 3rd	5.16e-2	0.76	3.02e-2	0.77	1.75e-2	0.78
Semi-Lagrangian HWENO 3rd	3.27e-2	0.78	1.89e-2	0.79	1.09e-2	0.80
Semi-Lagrangian WENO 5th	3.22e-2	0.83	1.80e-2	0.84	9.97e-3	0.85
Semi-Lagrangian HWENO 5th	2.94e-2	0.84	1.63e-2	0.85	8.99e-3	0.86

(a) Error between the exact solution and the approximated solutions

n_x	200	400	800
Semi-Lagrangian cubic spline	5.75e-1	5.12e-1	5.19e-1
Semi-Lagrangian WENO 3rd	5.13e-3	7.22e-3	1.11e-2
Semi-Lagrangian HWENO 3rd	5.71e-4	5.18e-4	4.37e-4
Semi-Lagrangian WENO 5th	1.93e-3	2.34e-3	3.43e-3
Semi-Lagrangian HWENO 5th	1.09e-3	1.42e-3	1.46e-3

(b) Error of total variation

TABLE 5. Comparison the semi-Lagrangian methods in discontinuous solution case: *(a) Error in L^1 norm and r is the order of accuracy (b) Error on the total variation. The final time is $T_{end} = 8$.*

n_x	200		400		800	
	$\|\cdot\|_1$	r	$\|\cdot\|_1$	r	$\|\cdot\|_1$	r
Finite difference WENO 5th	4.50e-2	0.83	2.53e-2	0.83	1.43e-2	0.82
Finite difference HWENO 5th	4.07e-2	0.83	2.29e-2	0.83	1.29e-2	0.83

(a) Error between the exact solution and the approximated solutions

n_x	200	400	800
Finite difference WENO 5th	9.54e-5	8.43e-5	6.58e-5
Finite difference HWENO 5th	2.30e-3	2.47e-3	1.88e-3

(b) Error of total variation

TABLE 6. Comparison of finite difference methods in discontinuous solution case: *(a) Error in L^1 norm and r is the order of accuracy (b) Error on the total variation. The final time is $T_{end} = 8$.*

We finally consider an oscillatory solution where the initial condition is given by [22],

$$f(0,x) = \begin{cases} \frac{1}{6}[G(x,z-\delta) + G(x,z-\delta) + 4G(x,z)], & \text{for } -0.8 \le x \le -0.6, \\ 1, & \text{for } -0.4 \le x \le -0.2, \\ 1-|10(x-0.1)|, & \text{for } 0 \le x \le 0.2, \\ \frac{1}{6}[F(x,z-\delta) + F(x,z-\delta) + 4F(x,z)], & \text{for } 0.4 \le x \le 0.6, \\ 0, & \text{otherwise.} \end{cases} \tag{5.3}$$

where $G(x,z) = \exp(-\beta(x-z)^2)$, $F(x,a) = \{\max((1-\alpha^2(x-a)^2)^{1/2},0)\}$ with $\alpha = 0.5$, $z = -0.7$, $\delta = 0.005$, $\alpha = 10$ and $\beta = (\log 2)/36\delta^2$.

We have similar observations of both regular solution and discontinuous solution cases in Figure 2. From table (e), we see that the usual semi-Lagrangian method with cubic spline interpolation is again the most precise method. It approximates well exponential function, but involves too much oscillation in step function. The other methods with WENO or HWENO reconstruction avoid a lot spurious oscillations. It seems that semi-Lagrangian methods is less dissipative than finite difference method, which can be seen in step function and peak function.

From [10], it is already known that classical Hermite reconstruction gives a better amplification coefficient than the one obtained using a Lagrange interpolation. For HWENO reconstruction, a rigorous analysis based on Fourier analysis has to be performed but is much more delicate since the scheme is nonlinear. We refer for instance to the works [23, 32].

5.3. **Simplified paraxial Vlasov-Poisson model.** We apply the numerical methods presented in previous sections to the following Vlasov-Poisson system satisfied by $f(t,r,v)$, where $r \in \mathbb{R}$, $v \in \mathbb{R}$ [4]

$$\begin{cases} \dfrac{\partial f}{\partial t} + \dfrac{v}{\varepsilon}\dfrac{\partial f}{\partial r} + \left(E_f - \dfrac{r}{\varepsilon}\right)\dfrac{\partial f}{\partial v} = 0, \\ \dfrac{1}{r}\dfrac{\partial}{\partial r}\left(rE_f\right) = \displaystyle\int_{\mathbb{R}} f\,dv. \end{cases} \tag{5.4}$$

The electric field can be expressed explicitly as follows

$$E_f(t,r) = \frac{1}{r}\int_0^r s\,\rho(t,s)\,ds,$$

where $\rho(t,r) = \int_{\mathbb{R}} f(t,r,v)dv$, hence we will compute E_f by a simple numerical integration.

The initial condition is chosen as a Gaussian in velocity multiplied by a regularized step function in r:

$$f_0(r,v) = \frac{4}{\sqrt{2\pi\alpha}}\chi(r)\exp(-\frac{v^2}{2\alpha}), \tag{5.5}$$

with $\chi(r) = \frac{1}{2}\mathrm{erf}(\frac{r+1.2}{0.3}) - \frac{1}{2}\mathrm{erf}(\frac{r-1.2}{0.3})$ and $\alpha = 0.2$. The Vlasov-Poisson system (5.4) conserves mass

$$\frac{d}{dt}\int_{\mathbb{R}^2} f(t,r,v)drdv = 0,$$

and also L^p norm for $1 \le p < \infty$

$$\frac{d}{dt}\|f(t,r,v)\|_{L^p(\mathbb{R}^2)} = 0.$$

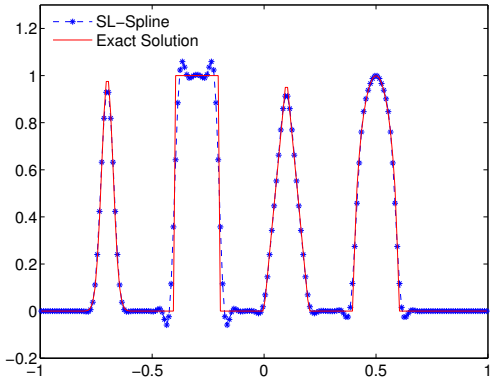

(a) Semi-Lagrangian cubic spline

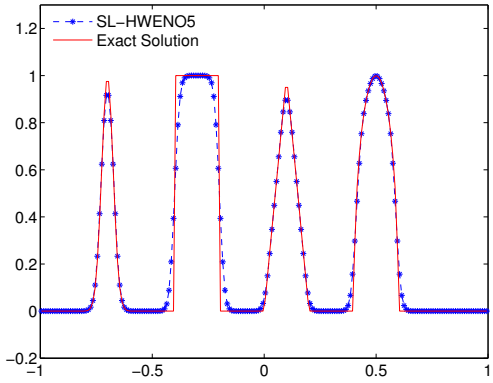

(b) Semi-Lagrangian-HWENO 5th

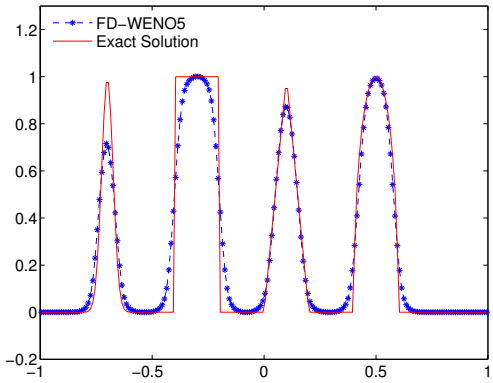

(c) Finite difference-WENO 5th

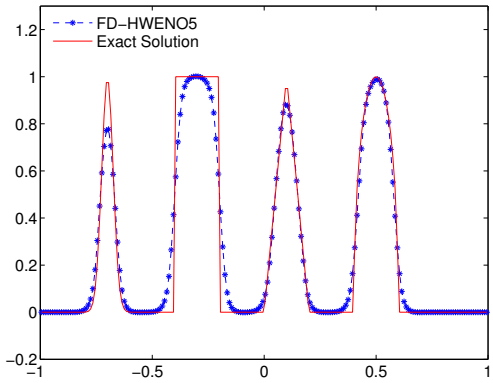

(d) Finite difference-HWENO 5th

SL-Spline	SL-HWENO5	FD-WENO5	FD-HWENO5
5.93e-2	6.95e-2	8.87e-2	7.66e-2

(e) Error in L^1 norm

FIGURE 2. Plot solutions of the linear equation (5.1) with initial data (5.3). $n_x = 200$, CFL= 2.5 for the semi-Lagrangian methods and CFL= 0.85 for the finite difference methods. The final time is $T_{\text{end}} = 8$.

Therefore, the evolution in time of these quantities will be observed for various numerical schemes. We will also investigate the time evolution of the kinetic energy of the Vlasov-Poisson system (5.4) :

$$\mathcal{E}(t) = \int_{\mathbb{R}^2} \frac{v^2}{2} f \, dr \, dv. \tag{5.6}$$

In the following we take the parameter $\varepsilon = 0.7$ and the computational domain is $(r, v) \in \Omega = [-4, 4]^2$.

Concerning the numerical resolution using semi-Lagrangian methods, we notice that we deliberately choose not to apply a time splitting in order to use this method in a general context. The characteristic curves corresponding to the Vlasov equation (5.4) cannot be solved explicitly. To compute the characteristic curves, we have multi-step method as the second order leap-frog scheme [30] or single time step method as the second order predictor-corrector scheme [3]. Finally, we interpolate the distribution function $f(r^n, v^n)$ by a tensor product for cubic spline or by a dimension by dimension Hermite WENO reconstruction.

Let us first compare the numerical methods for searching the characteristic curves. A reference solution of kinetic energy is computed using a fifth order finite difference WENO method with very fine mesh ($\Delta t = 1/1600$ and $n_x = 1025$). We denote the linear phase for

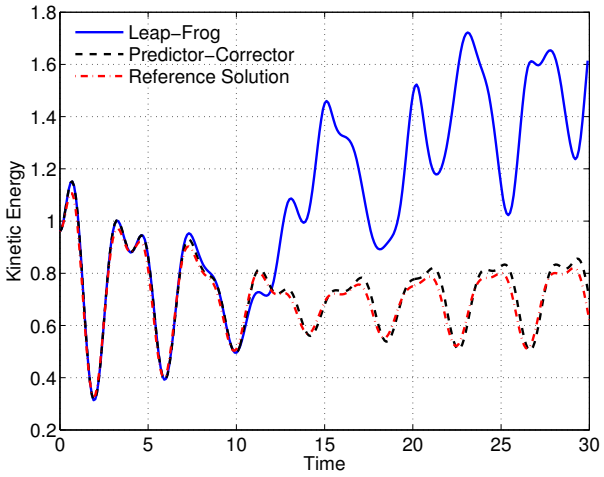

FIGURE 3. Comparison between the semi-Lagrangian methods with the Leap-Frog and Predictor-Corrector time integrators for Beam test. Mesh size is $n_x = 257$, $\Delta t = 1/100$.

time interval $t \leq 10$, and the nonlinear phase for time interval $t > 10$ where small filaments are generated. Figure 3 illustrates that the leap-frog scheme has a very bad kinetic energy for $t > 10$. It is because the leap-frog time integrator which decouples odd and even time steps and leads to a checker-board like instability that has been observed before [14]. At contrast, the predictor-corrector scheme has a kinetic energy close to reference solution.

From Figure 4, we observe that at time $t = 10$, the distribution function f of these two methods is similar, where two small filaments appear (see top of Figure 4). Then during the nonlinear phase, a large number of filaments are generated due to the non-linearity of the Vlasov-Poisson system and the distribution functions f obtained with leap-frog and predictor-corrector methods start to differ strongly at $t \geq 15$. At time $t \geq 20$, the leap-frog method generates a completely unstable beam. Therefore, in the sequel, the predictor-corrector scheme will be used for time integrator.

In Figure 5, we compare the evolution of invariants (mass, L^2 norm, minimum of the density) and the kinetic energy obtained from semi-Lagrangian and finite difference methods. Compared to the other methods, the semi-Lagrangian method with HWENO reconstruction has a very bad mass conservation in nonlinear phase (see Figure 5(a)). The semi-Lagrangian method with cubic spline interpolation has the best L^2 norm conservation. Moreover, for finite difference methods, the HWENO reconstruction has a better L^2 norm conservation than the WENO reconstruction, which indicates that HWENO reconstruction is less dissipative (see Figure 5(b)). The kinetic energy obtained with all these methods is relatively close in the linear phase $t < 10$, but it is slightly different in the nonlinear phase $t > 10$ (see Figure 5(c)). Finally, the semi-Lagrangian method with cubic spline interpolation has significant oscillation in nonlinear then the other methods (see Figure 5(d)).

These numerical simulations illustrate perfectly that semi-Lagrangian methods without splitting work well during the linear phase even with very large time step, but they are not appropriate during the nonlinear phase when micro-structures appear (filamentation). While the finite difference methods seems more suitable for nonlinear phase.

5.4. **Guiding center model.** We finally consider the guiding center model [21], which can be derived by integrating the 4D Drift-Kinetic model [19] with respect to variables $(z, v_\parallel)$.

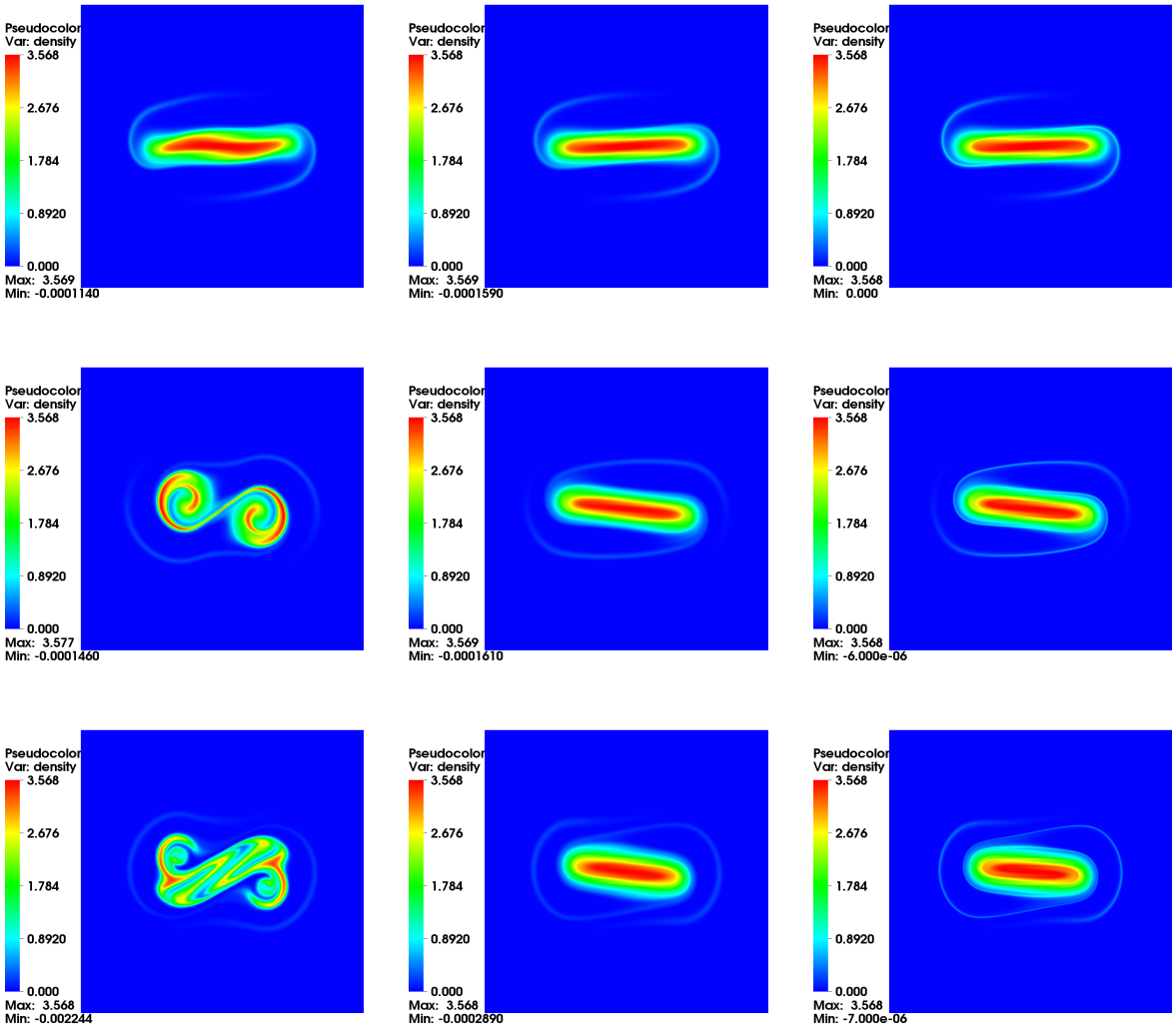

(a) (b) (c)

FIGURE 4. Distribution function for Beam test: (a) the Leap-frog scheme; (b) the Predictor-corrector scheme; (c) Reference solution at time $t = 10$, 15 and 20. The HWENO5 reconstruction is used for interpolation. Mesh size is $n_x = 257, \Delta t = 1/100$.

This model can describe highly magnetized plasma in the transverse plane, given by

$$\begin{cases} \frac{\partial \rho}{\partial t} + \mathbf{U} \cdot \nabla \rho = 0, \\ -\Delta \phi = \rho. \end{cases} \tag{5.7}$$

where the velocity $\mathbf{U} = (-\partial_y \phi, \partial_x \phi)$. Here we consider the model in a disk domain

$$D = \{(x, y) \in \mathbb{R}^2 : \sqrt{x^2 + y^2} \leq R\}$$

and assume that the electric potential is vanishing at the boundary

$$\phi(x, y) = 0, \quad (x, y) \in \partial D. \tag{5.8}$$

Then if we ignore the effect of boundary conditions, the guiding center model verifies the following properties :

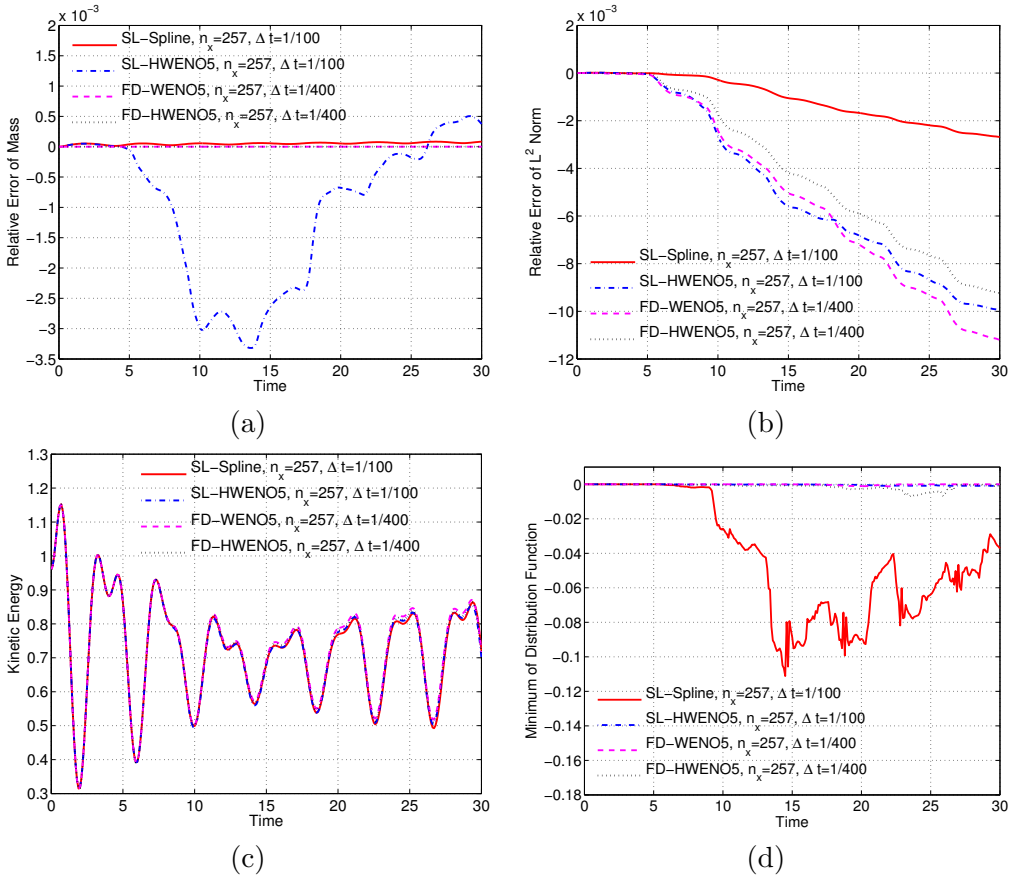

FIGURE 5. Comparison between the semi-Lagrangian with cubic spline, Hermite WENO 5th and the finite difference with Hermite WENO 5th methods for Beam test.

(1) Positivity of density ρ

$$0 \le \rho(t,x,y).$$

(2) Mass conservation

$$\frac{d}{dt}\left(\int_D \rho dxdy\right) = 0.$$

(3) L^p norm conservation, for $1 \le p \le \infty$

$$\frac{d}{dt}\|\rho\|_{L^p(D)} = 0.$$

(4) Energy conservation

$$\frac{d}{dt}\left(\int_D |\nabla\phi|^2 dxdy\right) = 0.$$

To solve the system (5.7), we use a scheme based on Cartesian mesh and apply an Inverse Lax-Wendroff procedure to treat boundary conditions on kinetic equations [12, 13]. Actually, this system has been already solved in polar coordinates in [21]. But, the change of coordinate usually produce an artificial singularity at the origin, which needs a particular treatment. At contrast, with the Inverse Lax-Wendroff technique on Cartesian mesh, we do not have any singularity and it is not related to the numerical scheme since boundary effects and numerical schemes are treated independently. Furthermore, it is easy to adapt to other geometries [12, 13].

In this section, we only focus on discretization of boundary condition (5.8) of Poisson equation. The one for transport equation is trivial, since a homogeneous Dirichlet boundary condition will be used.

5.4.1. *Discretization of Poisson equation.* A classical five points finite difference approximation is used to discretize the Poisson equation. However, to discretize the Laplacian operator $\Delta\phi$ near the physical boundary, we notice that some points of the usual five points finite difference formula can be located outside of interior domain. For instance, Figure 6 illustrates the discretization stencil for $\Delta\phi$ at the point (x_i, y_j). The point $\mathbf{x}_g = (x_i, y_{j-1})$ is located outside of interior domain. Let us denote the approximation of ϕ at the point $\mathbf{x}_g$ by $\phi_{i,j-1}$. Thus $\phi_{i,j-1}$ should be extrapolated from the interior domain.

We extrapolate $\phi_{i,j-1}$ on the normal direction $\mathbf{n}$

$$\phi_{i,j-1} = \tilde{w}_p\phi(\mathbf{x}_p) + \tilde{w}_h\phi(\mathbf{x}_h) + \tilde{w}_{2h}\phi(\mathbf{x}_{2h}), \tag{5.9}$$

where $\mathbf{x}_p$ is the cross point of the normal $\mathbf{n}$ and the physical boundary $\Omega_{\mathbf{x}_\perp}$. The points $\mathbf{x}_h$ and $\mathbf{x}_{2h}$ are equal spacing on the normal $\mathbf{n}$, *i.e.* $h = |\mathbf{x}_p - \mathbf{x}_h| = |\mathbf{x}_h - \mathbf{x}_{2h}|$, with $h = \min(\Delta x, \Delta y)$, Δx, Δy are the space steps in the directions x and y respectively. Moreover, $\tilde{w}_p$, $\tilde{w}_h$, $\tilde{w}_{2h}$ are the extrapolation weights depending on the position of $\mathbf{x}_g$, $\mathbf{x}_p$, $\mathbf{x}_h$ and $\mathbf{x}_{2h}$. In (5.9), $\phi(\mathbf{x}_p)$ is given by the boundary condition (5.8), whereas $\phi(\mathbf{x}_h)$, $\phi(\mathbf{x}_{2h})$ should be determined by interpolation.

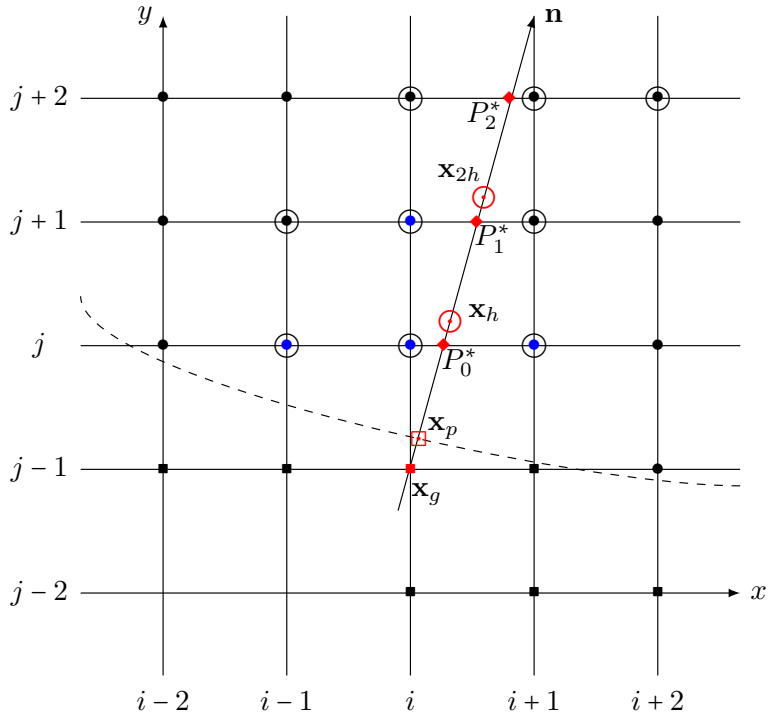

FIGURE 6. Spatially two-dimensional Cartesian mesh. • is interior point, ▪ is ghost point, ⊡ is the point at the boundary, ◯ is the point for extrapolation, the dashed line is the boundary.

For this, we first construct an interpolation stencil $\mathcal{E}$, composed of grid points of Ω. For instance, in Figure 6, the inward normal $\mathbf{n}$ intersects the grid lines $y = y_j$, y_{j+1}, y_{j+2} at points P_0^*, P_1^*, P_2^*. Then we choose the three nearest points of the cross point P_l^*, $l = 0, 1, 2$, in each line, *i.e.* marked by a large circle. From these nine points, we construct a Lagrange

polynomial $q_2(\mathbf{x}) \in \mathbb{Q}_2(\mathbb{R}^2)$ and evaluate the polynomial $q_2(\mathbf{x})$ at $\mathbf{x}_h$ and $\mathbf{x}_{2h}$, *i.e.*

$$\phi(\mathbf{x}_h) = \sum_{\ell=0}^{8} w_{h,\ell}\phi(\mathbf{x}_\ell),$$

$$\phi(\mathbf{x}_{2h}) = \sum_{\ell=0}^{8} w_{2h,\ell}\phi(\mathbf{x}_\ell),$$

with $\mathbf{x}_\ell \in \mathcal{E}$. Hence, we get $\phi_{i,j-1}$ which is approximated from the interior domain.

However, in some cases, we can not find a stencil of nine interior points. For instance, when the interior domain has small acute angle sharp, the normal $\mathbf{n}$ can not have three cross points P_l^*, $l = 0, 1, 2$ in interior domain, or we can not have three nearest points of the cross point P_l^*, $l = 0, 1, 2$, in each line. In this case, we alternatively use a first degree polynomial $q_1(\mathbf{x})$ with a four points stencil or even a zero degree polynomial $q_0(\mathbf{x})$ with an one point stencil. We can similarly construct the four points stencil or the one point stencil as above.

5.4.2. *Numerical simulation of the diocotron instability.* We now consider the diocotron instability for an annular electron layer [21, 25]. This plasma instability is created by two sheets of charge slipping past each other and is the analog of the Kelvin-Helmholtz instability in fluid mechanics. The initial data is given by

$$\rho_0(\mathbf{x}_\perp) = \begin{cases} (1 + \varepsilon\cos(\ell\theta))\exp\left(-4(r-6.5)^2\right), & \text{if } r^- \le \sqrt{x^2+y^2} \le r^+, \\ 0, & \text{otherwise,} \end{cases}$$

where ε is a small parameter, $\theta = \operatorname{atan2}(y, x)$. In the following tests, we take $\varepsilon = 0.01$, $r^- = 5$, $r^+ = 8$, $\ell = 7$.

We have seen in the previous section that semi-Lagrangian methods may be not very appropriate during the nonlinear phase. Indeed, on the one hand, the semi-Lagrangian method with cubic spline interpolation involves too much oscillations when small filaments appear; on the other hand, the semi-Lagrangian method with Hermite WENO reconstruction avoid the oscillations but loses the conservative properties of physical problems. Therefore, we propose to apply a mixed method based on the Hermite interpolation with a WENO reconstruction: we use the semi-Lagrangian method for the linear phase with large time step; then we apply the conservative finite difference scheme for nonlinear phase with small time step respecting CFL condition. The criterion to pass from semi-Lagrangian to finite difference methods is as follows

$$\left| \int_{\mathbb{R}^2} [\rho_h(t_n) - \rho_h(t_{n-1})]\, d\mathbf{x} \right| > h^3, \tag{5.10}$$

where h is the smallest space step.

A comparison between the semi-Lagrangian method with cubic spline interpolation and the mixed method for the diocotron instability is presented in Figures 7 and 8. For a fair comparison an adaptive time step is also applied to the semi-Lagrangian method with cubic spline interpolation. We first choose a CFL number $\lambda \approx 2$ during the linear phase, then λ will be changed to 0.5 according to (5.10) for the nonlinear phase and the number of points in space is $n_x = n_y = 256$.

Using the semi-Lagrangian method with cubic spline interpolation, the relative error of mass oscillates a lot during the nonlinear phase, while relative error for the mixed method is more stable (see Figure 7(a)). Unfortunately, kinetic energy conservation and relative error of L^2 norm for the mixed method are worse than that for the semi-Lagrangian method with cubic spline interpolation, but the price to pay is to generate a non negligible negative values. Indeed, the HWENO reconstruction allow to control spurious oscillations generate from the discontinuous initial data and small structures (see Figure 7(d)). Moreover, we notice that semi-Lagrangian method with cubic spline interpolation switches time step at $t \approx 40$, where

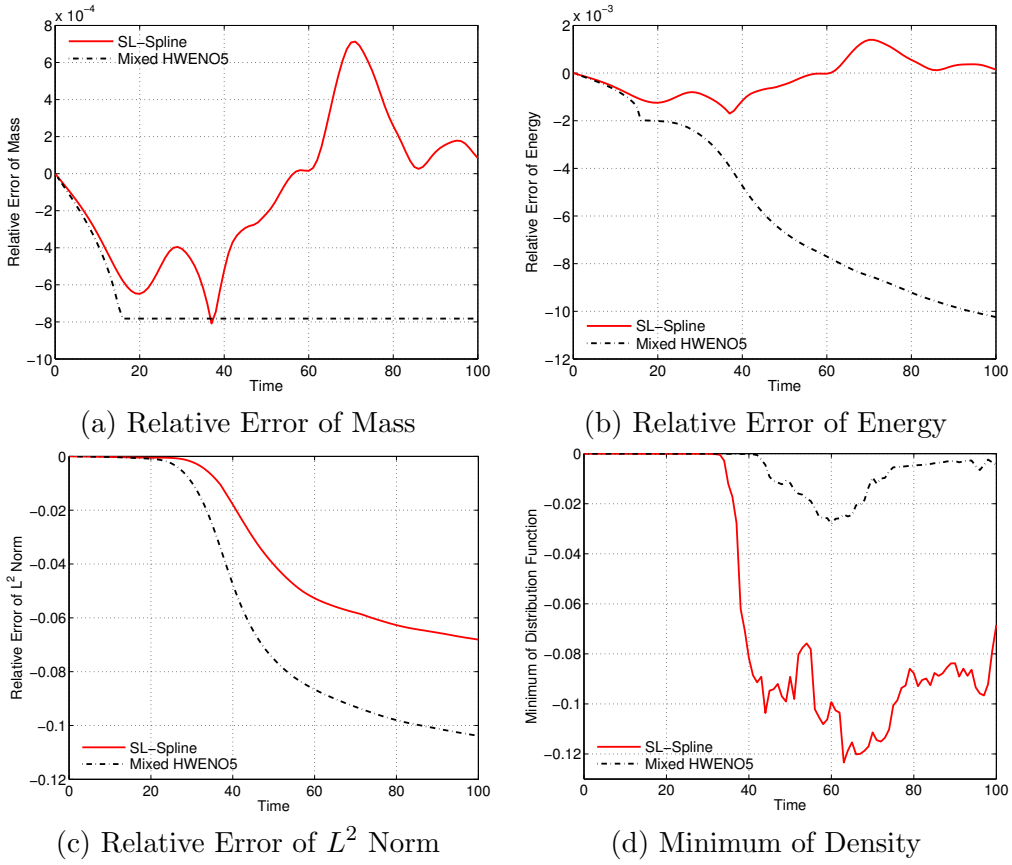

(a) Relative Error of Mass (b) Relative Error of Energy

(c) Relative Error of L^2 Norm (d) Minimum of Density

FIGURE 7. Guiding center model: Comparison between the semi-Lagrangian method with cubic spline interpolation and the mixed semi-Lagrangian/finite difference Hermite WENO5 method. Mesh size is $n_x = 256$. Adaptive time step is used.

the non negligible negative values are already generated, while the mixed HWENO method switches time step at the end of linear phase. Thus, although semi-Lagrangian method with cubic spline interpolation has better conservation laws in the linear phase of simulation, we propose to use mixed HWENO method in the whole period of simulation.

Finally, the evolution of the density ρ is presented in Figure 8. At first glance, we see the density of these two methods are very similar. At time $t = 30$, small filaments appear and then seven vortices are formed and move.

Looking more carefully, we observe that the numerical results obtained from the mixed method is a little bit more dissipative than the ones obtained from the semi-Lagrangian method with cubic spline interpolation, *i.e.* small structures of density are more thin. However, the semi-Lagrangian method is much more oscillatory than the mixed method, which can be observed from the minimum or maximum of density.

As a conclusion, although the semi-Lagrangian method with cubic spline interpolation is less dissipative than the mixed HWENO method, it involves too much numerical instabilities in nonlinear phase. Therefore, the mixed method controlling spurious oscillations is more appropriate for long time simulation in plasma physics.

6. Conclusion and perspective

In this paper, we have first developed a Hermite weighted essentially non-oscillatory reconstruction for semi-Lagrangian method and finite difference method respectively.

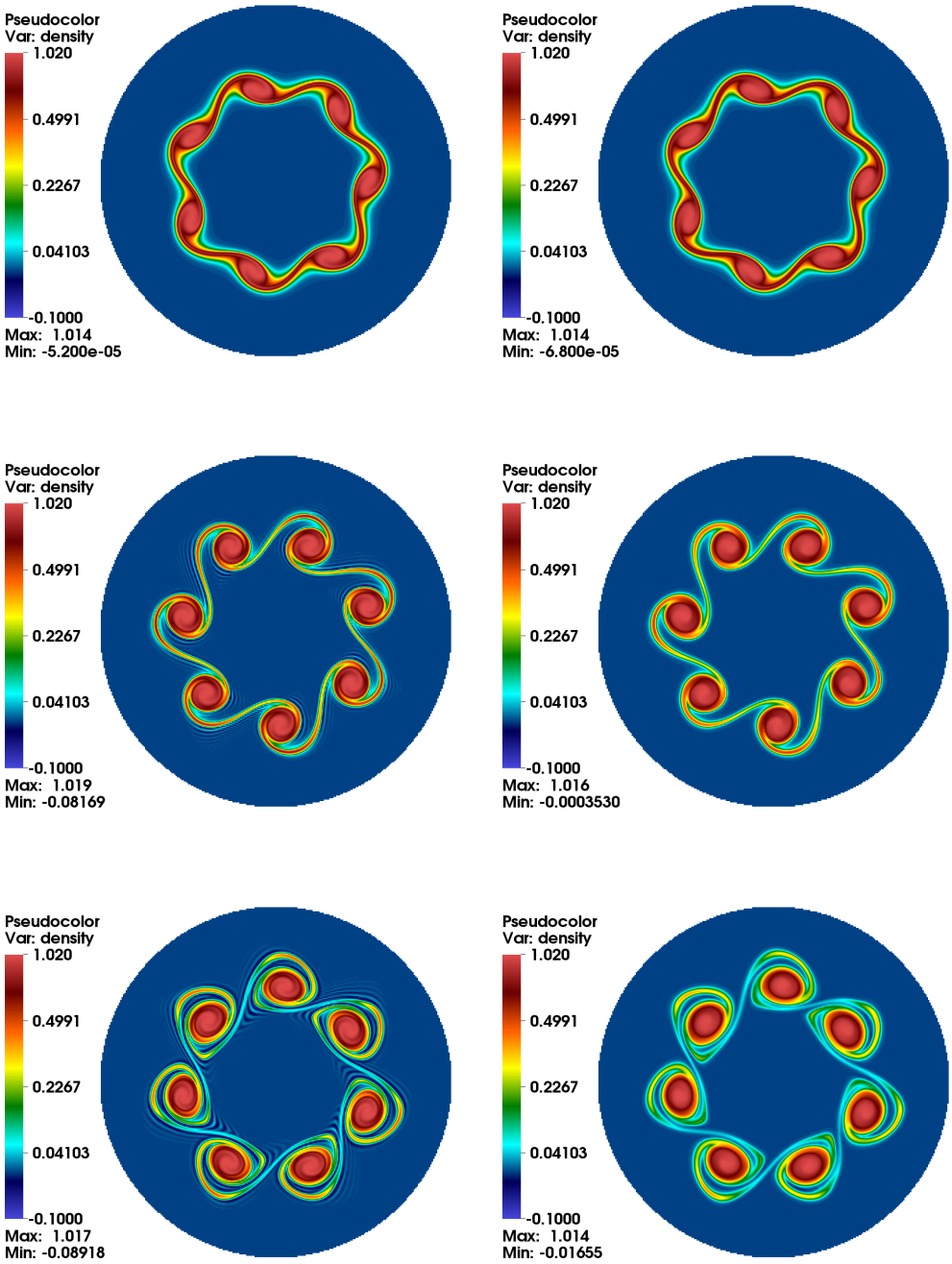

(a) (b)

FIGURE 8. Guiding center model. (a) the semi-Lagrangian method with cubic spline interpolation (b) the mixed semi-Lagrangian/finite difference method with Hermite WENO5 at time $t = 30$, 40 and 50.

We illustrate that such a reconstruction is less dissipative than usual weighted essentially non-oscillatory reconstruction. Then we have compared our approaches with the usual semi-Lagrangian method with cubic spline interpolation and finite difference method with WENO reconstruction. The both semi-Lagrangian methods are efficient and accurate for linear phase

even with a large time step, however, the one with cubic spline interpolation involves too much non negligible oscillation in nonlinear phase, while the one with HWENO reconstruction becomes dissipative.

The finite difference method is stable under the classical CFL condition, but it is much more stable in nonlinear phase and it conserves mass. We thus apply a mixed method using the semi-Lagrangian method in linear phase and finite difference method during the nonlinear phase, called mixed HWENO5 method.

We finally apply the mixed HWENO5 method to the simulation of the diocotron instability and observe that although the mixed HWENO5 method is a little more dissipative than the semi-Lagrangian method with cubic spline interpolation, but it is much more stable during the nonlinear phase.

The next step is now to apply our mixed method to more realistic and high dimensional plasma turbulence simulations, for instance, 4D Drift-Kinetic simulation [16] or 5D Gyrokinetic simulation[15].

Acknowledgment

The authors are partially supported by the European Research Council ERC Starting Grant 2009, project 239983-*NuSiKiMo* and the Inria project Kaliffe.

References

[1] A. J. Brizard and T.S Hahm, Foundations of nonlinear gyrokinetic theory, *Review of Modern Physics* **79** (2007), pp. 421–68.

[2] C. Z. Cheng and G. Knorr, The integration of the Vlasov equation in configuration space, *Journal of Computational Physics*, **22** (1976), pp. 330–351.

[3] N. Crouseilles, M. Mehrenberger, E. Sonnendrucker, Conservative semi-Lagrangian schemes for Vlasov equations, *Journal of Computational Physics* **229** (2010), pp. 1927–1953.

[4] N. Crouseilles, M. Lemou, F. Méhats, Asymptotic preserving schemes for highly oscillatory, *Journal of Computational Physics*, **248** (2013), pp. 287–308.

[5] N. Crouseilles, A. Ratnani, E. Sonnendrücker, An Isogeometric Analysis approach for the study of the gyrokinetic quasi-neutrality equation, *Journal of Computational Physics*, **231** (2012), pp. 373–393.

[6] B. Després, Stability of high order finite volume schemes for the 1D transport equation, *In Finite volumes for complex applications V*, pp. 337–342. ISTE, London, 2008.

[7] B.A. de Dios, J.A. Carrillo and C.W. Shu, Discontinuous Galerkin methods for the multidimensional Vlasov-Poisson problem, *Mathematical Models and Methods in Applied Sciences*, **22** (2012), 1250042.

[8] M.R. Feix, P. Bertrand, A. Ghizzo, Eulerian codes for the Vlasov equation, *Series on Advances in Mathematics for Applied Sciences, Kinetic Theory and Computing*, **22** (1994), pp. 45–81.

[9] F. Filbet, E. Sonnendrücker, P. Bertrand, Conservative numerical schemes for the Vlasov equation, *Journal of Computational Physics*, **172** (2001), pp. 166–187.

[10] F. Filbet, E. Sonnendrücker, Comparison of Eulerian Vlasov solvers, *Computer Physics Communications*, **150** (2003), 247–266.

[11] F. Filbet, E. Sonnendrücker, Modeling and numerical simulation of space charge dominated beams in the paraxial approximation, *Mathematical Models & Methods in Applied Sciences*, **16** (2006), 763–791.

[12] F. Filbet and C. Yang, An inverse Lax-Wendroff method for boundary conditions applied to Boltzmann type models, *Journal of Computional Physics*, **245** (2013), pp. 43–61.

[13] F. Filbet and C. Yang, Numerical Simulations of Kinetic Models for Chemotaxis, *SIAM Journal on Scientific Computing*, 36(3) (2014) : B348-B366.

[14] A. Ghizzo, P. Bertrand, M. Shoucri, T.W. Johnston, E. Filjakow, M.R. Feix, A Vlasov code for the numerical simulation of stimulated Raman scattering, *Journal of Computional Physics*, **90** (1990), pp. 431–453.

[15] X. Garbet, Y. Idomura, L. Villard and T.H. Watanabe, Gyrokinetic simulations of turbulent transport, *Nuclear Fusion*, **50** (2010), 043002.

[16] V. Grandgirard, M. Brunetti, P. Bertrand, N. Besse, X. Garbet, P. Ghendrih, G. Manfredi, Y. Sarazin, O. Sauter, E. Sonnendrücker, J. Vaclavik, L. Villard, A drift-kinetic semi-Lagrangian 4D code for ion turbulence simulation, *Journal of Computational Physics*, **217** (2006), pp. 395–423.

[17] V. Grandgirard, Y. Sarazin, X. Garbet, G. Dif-Pradalier, P. Ghendrih, N. Crouseilles, G. Latu, E. Sonnendrücker, N. Besse, Computing ITG turbulence with a full-f semi-Lagrangian code,*Communications in Nonlinear Science and Numerical Simulation*, **13** (2008), pp. 81–87.
[18] W. Guo and J.-M. Qiu, Hybrid semi-Lagrangian finite element-finite difference methods for the Vlasov equation, *Journal of Computational Physics*, **234** (2013), pp. 108–132.
[19] R.D. Hazeltine, Recursive derivation of drift-kinetic equation, *Plasma Physics*, **15** (1973), pp. 77–80.
[20] R. E. Heath, I. M. Gamba, P.J. Morrison and C. Michler, A discontinuous Galerkin method for the Vlasov-Poisson system, *Journal of Computational Physics*, **231** (2012), pp. 1140–1174.
[21] S. Hirstoaga, E. Madaule, M. Mehrenberger and J. Pétri, Semi-Lagrangian simulations of the diocotron instability, submitted.
[22] G.-S. Jiang and C.-W. Shu, Efficient implementation of weighted ENO schemes, *Journal of computational physics*, **126** (1996), pp. 202-228.
[23] S.Y. Lin and J.J. Hu, Parametric study of weighted essentially nonoscillatory schemes for computational aeroacoustics, *AIAA Journal*, **39** (2001), pp. 371–379.
[24] T. Nakamura and T. Yabe, Cubic interpolated propagation scheme for solving the hyper-dimensional Vlasov-Poisson equation in phase space, *Computer Physics Communications*, **120** (1999), pp. 122–154.
[25] J. Pétri, Non-linear evolution of the diocotron instability in a pulsar electrosphere: 2D PIC simulations, *Astronomy & Astrophysics*, **503** (2009), pp. 1–12.
[26] J. Qiu, Chi-Wang Shu, Hermite WENO schemes and their application as limiters for Runge-Kutta discontinuous Galerkin method: one-dimensional case, *Journal of Computational Physics*, **193** (2004), pp. 115–135.
[27] J. M. Qiu and A. Christlieb, A conservative high order semi-Lagrangian WENO method for the Vlasov equation. *Journal of Computational Physics*, **229** (2010), pp. 1130–1149.
[28] J. M. Qiu, C.-W. Shu, Conservative high order semi-Lagrangian finite difference WENO methods for advection in incompressible flow. *Journal of Computational Physics*, **230** (2011), pp. 863–889.
[29] J. M. Qiu and C.-W. Shu, Positivity preserving semi-Lagrangian discontinuous Galerkin formulation: theoretical analysis and application to the Vlasov-Poisson system, *Journal of Computational Physics*, **230** (2011), pp. 8386–8409.
[30] E. Sonnendrücker, J. Roche, P. Bertrand, A. Ghizzo, The semi-Lagrangian method for the numerical resolution of Vlasov equation, *Journal of Computational Physics*, **149** (2013), pp. 201–220.
[31] T. Umeda, Y. Nariyuki, D. Kariya, A non-oscillatory and conservative semi-Lagrangian scheme with fourth-degree polynomial interpolation for solving the Vlasov equation, *Computer Physics Communications*, **183** (2012), pp. 1094–1100.
[32] Z.J. Wang and R.F. Chen, Optimized weighted essentially nonoscillatory schemes for linear waves with discontinuity, *Journal of Computational Physics*, **174** (2001), pp. 381–404.